Polymer Journal (2019) 51:1037–1044
https://doi.org/10.1038/s41428-019-0218-z

ORIGINAL ARTICLE

Preparation of polybenzoxazole–silica hybrid membranes for CO_2/CH_4 separation

Tomoyuki Suzuki[1] · Azumi Saito[1]

Received: 12 April 2019 / Revised: 17 May 2019 / Accepted: 20 May 2019 / Published online: 5 June 2019

Abstract

The gas transport properties of novel polybenzoxazole (PBO)–silica hybrid membranes prepared via a sol–gel reaction and different thermal treatment protocols were investigated. The thermal decomposition and glass transition temperatures of the hybrids increased with increasing silica content, indicating improved thermal stability by hybridization with silica. With increasing silica content and higher thermal treatment temperature, the hybrids showed enhanced CO_2 permeability and CO_2/CH_4 selectivity, which tended to intersect with the upper-bound trade-off line. The improved CO_2/CH_4 separation ability of the PBO–silica hybrid membranes might be due to the increased intermolecular chain distance and free volume holes favorable for CO_2/CH_4 separation created around the polymer/silica interfacial area.

Introduction

In the last few decades, gas separation with polymeric membranes has been an active field of research and industrial application [1–3]. Membrane-based gas separation is advantageous due to its low capital and operating costs, high energy efficiency, and ease of operation when compared to conventional separation processes such as pressure-swing adsorption, chemical absorption, and cryogenic distillation [4–6]. In general, the investigation of polymeric gas separation membranes focuses on the development of novel materials with high combinations of gas permeation and separation abilities. Polyimides (PIs) [7–10] and polybenzoxazoles (PBOs) [11–13], classified as rigid-rod aromatic polymers, have been widely studied as promising materials for high-performance gas separation membranes because of their high gas permselectivities, as well as outstanding thermal and mechanical properties. Recently, PI and PBO membranes containing inorganic compounds, called mixed matrix membranes (MMMs), have become of interest for the improvement of the gas transport properties of pristine PIs and PBOs [14–16]. In our previous study, it has been reported that PI–silica hybrid membranes prepared via a sol–gel reaction with alkoxysilanes possess controlled gas permselectivity, suggesting that free volume holes created around the polymer/silica interfacial area can be tuned to achieve desired gas permselectivities [17]. In addition, it has been found that PBO–silica hybrid membranes also show improved CO_2/CH_4 separation ability with increasing silica content [18, 19]. To our knowledge, however, there are few experimental reports regarding the gas transport properties of PBO–silica hybrid membranes with different molecular structures.

In this study, novel PBO–silica hybrid membranes with different molecular structures were prepared, and their gas transport properties were investigated. The PBO was derived from isophthaloyl chloride (IPC) instead of 4,4′-oxybis(benzoic acid chloride) studied previously [19] and 2,2-bis(3-amino-4-hydroxyphenyl)hexafluoropropane (6FAHP). In addition, several thermal treatment temperatures were also attempted at the stage of membrane preparation because an increased treatment temperature would bring about improved gas permeability of the PBOs due to an enhanced interchain distance and fractional free volume (FFV) [19, 20]. With the simultaneous application of hybridization and thermal treatment techniques, developments of PBO-based high-performance gas separation membranes with favorable gas permeability and/or selectivity would be expected.

✉ Tomoyuki Suzuki
suzuki@kit.ac.jp

[1] Faculty of Materials Science and Engineering, Kyoto Institute of Technology, Matsugasaki, Sakyo-ku, Kyoto 606-8585, Japan

Experimental

Materials

6FAHP, IPC, and tetraethoxysilane (TEOS) were purchased from Tokyo Chemical Industry Co., Ltd. (Tokyo, Japan). *N, O*-Bis(trimethylsilyl)acetamide (BSA), as an amide-type silylation agent, was obtained from Sigma-Aldrich (Tokyo, Japan). The coupling agent 3-(triethoxysilyl)propylsuccinic anhydride (TEOSPSA) and the solvent *N,N*-dimethylacetamide (DMAc) were supplied by AZmax Co. (Tokyo, Japan) and Nacalai Tesque, Inc. (Kyoto, Japan), respectively. These regents and solvent were used as received. Chemical structures of the monomers are shown in Fig. 1.

Polymerization

Poly(*o*-hydroxy amide) (PHA) as a precursor was synthesized by the in situ silylation method described as follows [21, 22]: 5 mmol of 6FAHP was dissolved in 10 ml of DMAc in a 50-ml three-necked flask under N_2 flow. To this solution, 20 mmol of BSA was added with stirring at room temperature, and the solution was stirred for 1 h. Next, the solution was cooled with an iced ethanol bath at 0–5 °C, and 4.85 mmol of IPC was added with stirring. The mixture was kept stirring at 0–5 °C for 1 h and then at room temperature for 3 h under N_2 flow. The resulting polymer solution was poured into distilled water. The precipitated polymer was collected and washed thoroughly with distilled water, followed by vacuum drying at 90 °C for 4 h. Finally, the solid PHA of amine-terminated 6FAHP-IPC, PHA(6FAHP-IPC), was obtained. A schematic representation of the synthesis of the PHA(6FAHP-IPC) is shown in Fig. 2.

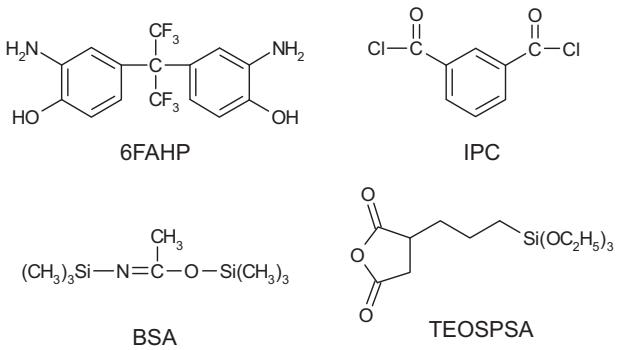

Fig. 1 Chemical structures of monomers

Membrane formation

In 5 ml of DMAc, 0.5 g of PHA(6FAHP-IPC) was dissolved, and 0.05 g of TEOSPSA was added with stirring. To this solution, appropriate amounts of TEOS, distilled water, and a catalytic amount of diluted hydrochloric acid were added, and the reaction mixture was stirred overnight. Next, the clear, homogeneous mixture was cast on a PET sheet and dried at 90 °C for 1 h in a heating oven to form a thin membrane. The prepared membrane was peeled off and fixed between two window-opened metal frames, and subsequently it was dehydro-cyclized and hybridized by the following stepwise heating in a heating oven under N_2 flow: (1) 100 °C for 1 h, (2) 200 °C for 1 h, and (3) a selected temperature of 400, 420, or 450 °C for 1 h. By controlling the mixture composition and thermal treatment temperature, the specified 6FAHP-IPC polybenzoxazole (PBO(6FAHP-IPC))–silica (SiO_2) hybrid membranes were obtained.

Measurements

Attenuated total reflection Fourier transform infrared (ATR FT-IR) spectra were recorded by an FT/IR-4100 equipped with an ATR PRO ONE (ZnSe prism) (JASCO Corp., Japan) over a wavenumber range of 550–4000 cm^{-1} and with a resolution of 2 cm^{-1}. Scanning electron microscopy (SEM) images were acquired using a VE-7800 (Keyence

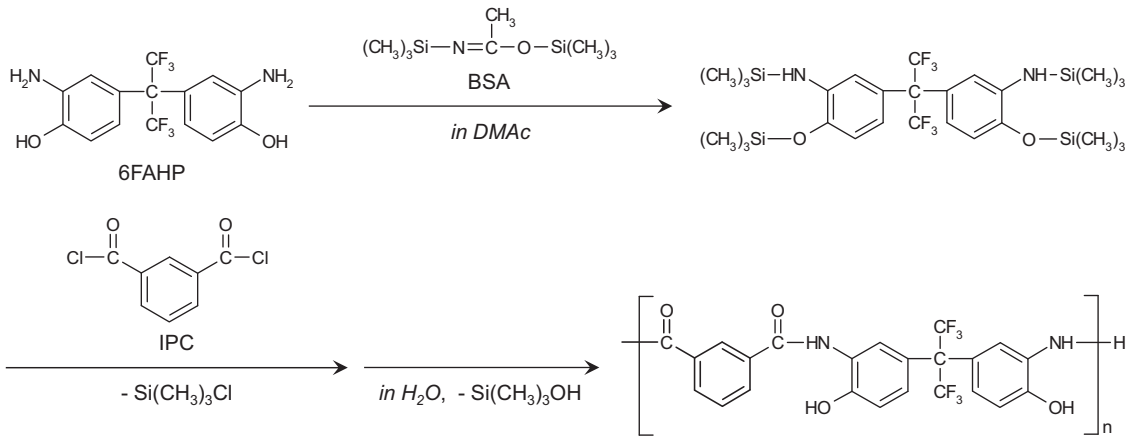

Fig. 2 Schematic representation of the synthesis of PHA(6FAHP-IPC)

Corp., Japan) at an accelerating voltage of 10 kV. Samples for the SEM analyses were coated using an E-1010 ion sputter coater (Hitachi High-Technologies Corp., Japan) with a platinum target. Differential scanning calorimetry (DSC) measurements were carried out with a DSC-60 (Shimadzu Corp., Japan) at a heating rate of 10 °C/min and a temperature range of 25–400 °C under N_2 flow. Thermogravimetric analysis (TGA) experiments were performed with a DTG-60 (Shimadzu Corp., Japan) at a heating rate of 10 °C/min over a temperature range of 25–800 °C under N_2 or air flow. CO_2, O_2, N_2, and CH_4 permeation measurements were carried out with a constant volume/variable pressure apparatus at 76cmHg and 25 °C. The gas permeability coefficient, P (barrer, 1 barrer $= 1 \times 10^{-10}$ cm^3 (STP)cm/cm^2 s cmHg), was calculated by the following equation [23]:

$$P = \left[\frac{273}{T} \cdot \frac{V}{A} \cdot L \cdot \frac{1}{p} \cdot \frac{1}{76} \cdot \frac{\mathrm{d}p}{\mathrm{d}t}\right] \times 10^{10} \quad (1)$$

where T is the absolute temperature (K), V is the downstream volume (cm^3), A is the membrane area (cm^2), L is the membrane thickness (cm), p is the upstream pressure (cmHg), and dp/dt is the permeation rate (cmHg/s). The gas permeability coefficient can be explained on the basis of the solution-diffusion mechanism, which is represented by the following equation [24, 25]:

$$P = D \times S \quad (2)$$

where D (cm^2/s) is the diffusion coefficient and S (cm^3 (STP)/cm$^3_{\mathrm{polym}}$.cmHg) is the solubility coefficient. The diffusion coefficient was determined by the time-lag method represented by the following equation [26]:

$$D = \frac{L^2}{6t} \quad (3)$$

where t (s) is the time lag. Wide-angle X-ray scattering (WAXS) patterns were recorded by an MX-Labo (Mac Science Co., Ltd.) using Cu-Kα radiation with a wavelength of $\lambda = 1.54$ Å. The scan range was from 10° to 25° under a voltage of 40 kV and a current of 18 mA. The average d-spacing, d (Å), was determined based on Bragg's law [20]:

$$n\lambda = 2d \sin\theta \quad (4)$$

where n is the integer, λ denotes the X-ray wavelength, and θ indicates the diffraction angle. A floating method was used for measuring the density of pristine PBO(6FAHP-IPC) membranes prepared by different thermal treatment protocols with NaBr aqueous solution at 25 °C. According to the group contribution method, the FFV of a polymer can be estimated by the following equations [27, 28]:

$$\mathrm{FFV} = \frac{V_{\mathrm{sp}} - 1.3V_w}{V_{\mathrm{sp}}} \quad (5)$$

$$V_{\mathrm{sp}} = \frac{M}{\rho} \quad (6)$$

where V_{sp} (cm^3/mol) is the specific molar volume, V_w (cm^3/mol) is the van der Waals volume of the repeating unit, M (g/mol) is the molecular weight of the repeating unit, and ρ (g/cm^3) is the experimental density.

Results and discussion

Membrane characterization

Figure 3 shows ATR FT-IR spectra of PHA(6FAHP-IPC) and 400 °C-treated PBO(6FAHP-IPC)–silica hybrid membranes. For the PHA(6FAHP-IPC), as a precursor polymer, the bands assigned to amide linkages are found at ~1510 (N–H bending) and 1650 cm^{-1} (C=O stretching) [20, 29]. On the other hand, for the PBO(6FAHP-IPC) and its silica hybrids, the bands attributed to the amide linkages mentioned above disappeared, and new absorption bands at 846 (benzoxazole ring), 1049 (phenyl–O–C stretching), 1478 (benzoxazole ring), and 1629 cm^{-1} (C=N stretching), which are typical bands of PBO [12, 20, 30, 31], appeared. This fact indicates that the PHA is converted into PBO by

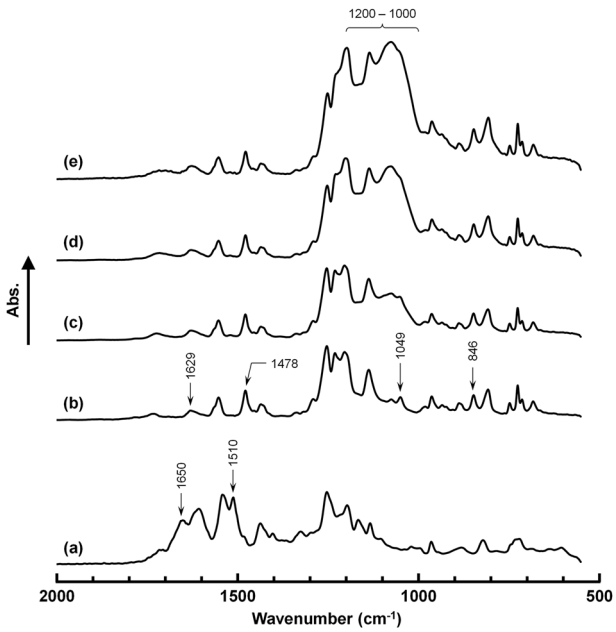

Fig. 3 ATR FT-IR spectra of **a** PHA(6FAHP-IPC) and **b**–**e** 400 °C-treated PBO(6FAHP-IPC)–silica hybrid membranes; silica content: **b** 0, **c** 10, **d** 20, and **e** 30 wt%

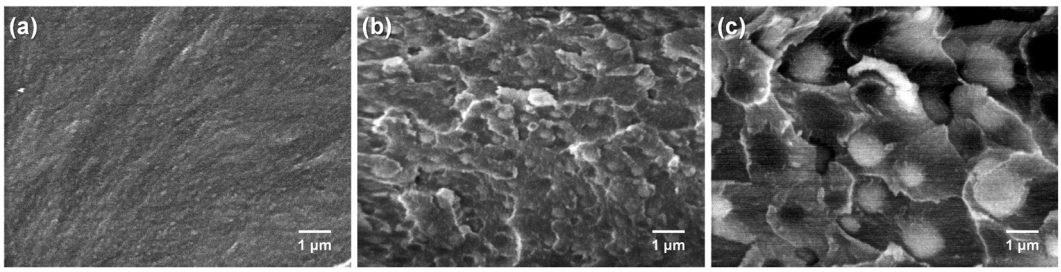

Fig. 4 Cross-sectional SEM images of 400 °C-treated PBO(6FAHP-IPC)–silica hybrid membranes; silica content: **a** 10, **b** 20, and **c** 30 wt%

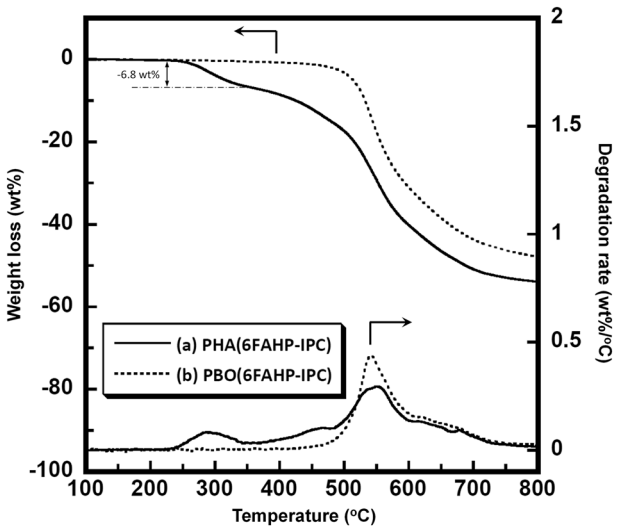

Fig. 5 Thermogravimetric and differential thermogravimetric curves of **a** PHA(6FAHP-IPC) and **b** 400 °C-treated PBO(6FAHP-IPC) membranes obtained under N_2 flow conditions

the established thermal treatment protocol. For the PBO (6FAHP-IPC)–silica hybrids, a strong absorption band at ~1000–1200 cm^{-1} assigned to Si–O–Si asymmetric stretching [32, 33] is also observed, and the intensity of the band increases with increasing silica content. This result indicates that the sol–gel reaction successfully progressed during the membrane preparation process, and a robust Si–O–Si network structure is formed in the hybrids. Similar results were obtained for the 420 °C- and 450 °C-treated hybrids (data not shown). Figure 4 represents cross-sectional SEM images of the 400 °C-treated PBO(6FAHP-IPC)–silica hybrids. As shown in Fig. 4, well-dispersed silica particles exist in the hybrid membranes, and it is found that increasing the silica content brings about an enlargement of the mean size of the silica particles.

The thermal properties of the PBO(6FAHP-IPC) and its silica hybrids were investigated. Figure 5 shows thermogravimetric and differential thermogravimetric curves of pristine PHA(6FAHP-IPC) and 400 °C-treated PBO (6FAHP-IPC) obtained under N_2 flow conditions. The PHA (6FAHP-IPC) was dried at 200 °C for 1 h to remove residual DMAc in the membrane prior to the TGA measurement [34]. For the PHA(6FAHP-IPC), a two-step weight loss is observed, and the first step in the range of 240 to 350 °C provides 6.8 wt% of the weight loss. The experimental weight loss is roughly in agreement with the expected weight loss caused by the removal of H_2O during the dehydro-cyclization of PHA(6FAHP-IPC) into PBO (6FAHP-IPC) (7.2 wt%). On the other hand, for the PBO (6FAHP-IPC), the first step of weight loss disappeared, and thermal decomposition initiates at ~500 °C, which corresponds to the second step of weight loss for the PHA (6FAHP-IPC). From the results of TGA measurements, it is again confirmed that the PHA(6FAHP-IPC) is successfully converted into the PBO(6FAHP-IPC) by the established oxazolization protocol. The 5% weight-loss temperature (T_d^5) and silica content of the 400 °C-treated hybrids were determined by the TGA measurements under air flow, and the obtained results are summarized in Table 1, in addition to glass transition temperature (T_g) measured by DSC analysis. It is confirmed from the residual at 800 °C that all hybrid membranes contain appropriate amounts of silica as expected. The T_g and T_d^5 values of the hybrid membranes increase with increasing silica content, indicating increased thermal stability and the restriction of molecular mobility of the PBO matrix by hybridization with silica.

Table 1 Thermal properties of 400 °C-treated PBO(6FAHP-IPC)–silica hybrid membranes

SiO_2 content (wt%)	T_g (°C)	T_d^5 in air (°C)	Residual at 800 °C (wt%)
0	340	507	–
10	343	510	9
20	349	516	24
30	353	521	34

Gas transport properties

Gas permeability, diffusivity, and solubility

The gas permeability, diffusion, and solubility coefficients of the PBO(6FAHP-IPC)–silica hybrids prepared with different thermal treatment protocols are summarized in Table 2. Unfortunately, we could not carry out the

Table 2 Gas transport properties, FFV, and *d*-spacing of PBO(6FAHP-IPC)–silica hybrid membranes measured at 25 °C

Preparation temperature (°C)	SiO_2 content (wt%)	*P* (barrer)				$D \times 10^8$ (cm^2/s)				$S \times 10^2$ ($cm^3(STP)/cm^3_{polym}cmHg$)				*d*-spacing (Å)	FFV
		CO_2	O_2	N_2	CH_4	CO_2	O_2	N_2	CH_4	CO_2	O_2	N_2	CH_4		
400	0	50	10	1.9	0.95	1.9	5.0	1.3	0.18	26	2.1	1.4	5.2	6.55	0.180
	10	62	12	2.3	1.2	2.6	7.6	1.6	0.27	24	1.6	1.4	4.5		
	20	83	16	2.9	1.5	2.7	8.5	1.9	0.27	31	1.9	1.5	5.4		
	30	137	24	4.7	2.4	3.5	11	2.6	0.40	39	2.2	1.8	6.0		
420	0	66	14	2.6	1.3	2.2	6.2	1.7	0.24	30	2.2	1.5	5.6	6.60	0.184
	10	90	17	3.2	1.8	3.2	8.2	2.1	0.35	28	2.0	1.5	5.1		
	20	165	30	6.1	3.4	4.5	13	3.3	0.55	36	2.3	1.9	6.3		
	30	220	39	7.9	4.0	5.0	14	3.6	0.57	46	2.7	2.2	7.1		
450	0	289	53	12	7.9	7.4	19	4.7	0.83	39	2.9	2.5	9.5	6.65	0.192
	10	428	70	16	11	11	24	6.3	1.2	40	2.9	2.5	9.2		
	20	563	87	21	14	14	30	8.6	1.7	41	3.0	2.5	8.4		

permeation measurements for the 450 °C-treated hybrid containing 30 wt% silica due to the shrinkage-induced breaking of the membranes during the cooling process of membrane formation.

From the overview of the effect of hybridization with silica, it is indicated that the gas permeability of the hybrids increases with increasing silica content, mainly in connection with increased gas diffusivity. Similar enhancements of gas permeability and/or diffusivity have been reported for PI–silica nanocomposites, in which the addition of silica nanoparticles into a PI matrix facilitates the formation of nanogaps around the interface between nanoparticles and polymer chain segments, resulting in highly enhanced gas permeability [35, 36]. Similar to another study regarding positron annihilation lifetime spectroscopy analyses of polyimide-based MMMs, it has been discovered that the incorporation of inorganic nanoparticles accelerates the additional formation of free volume holes, which leads to increased gas diffusivity and, as a consequence, increased gas permeability for the MMMs [37]. Therefore, the increased gas permeability attributed to the increased gas diffusivity of the hybrids might be caused by the formation of free volume holes around the polymer/silica interfacial area.

The thermal treatment temperature also affects the gas transport properties of the PBO(6FAHP-IPC) and its silica hybrids. As shown in Table 2, the gas permeability and diffusivity increase with increasing thermal treatment temperature. Figure 6 represents the WAXS patterns of pristine PBO(6FAHP-IPC)s prepared by different thermal treatment protocols, and the *d*-spacing values calculated from Eq. (4) are listed in Table 2, in addition to FFV values obtained from equations (5) and (6). Both the *d*-spacing attributed to the intermolecular chain distance and FFV increase with increasing thermal treatment temperature. Wang et al. have reported that for a PBO, an increased treatment temperature brings about enlargement of the interchain distance and mean size of the free volume holes, which leads to enhanced gas permeability [11, 20]. The improved gas permeability and diffusivity of the PBO(6FAHP-IPC) and its silica hybrids with increasing treatment temperature are, therefore, attributed to the enlarged intermolecular chain distance and FFV. Especially for the hybrids, the gas permeability and diffusivity are efficiently improved by the effects of both hybridization with silica and an increased treatment temperature.

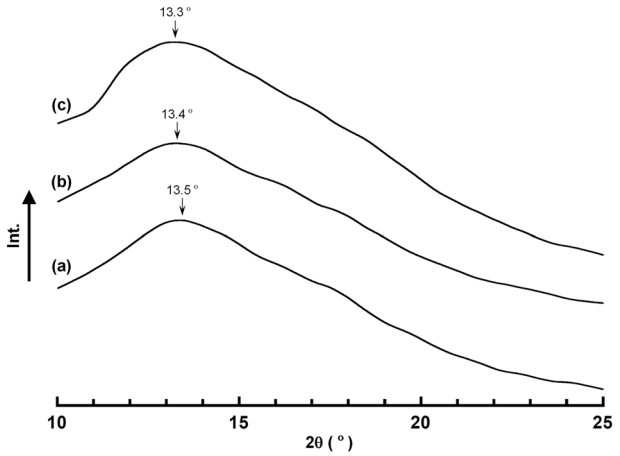

Fig. 6 WAXS patterns of pristine PBO(6FAHP-IPC) membranes treated at **a** 400 °C, **b** 420 °C, and **c** 450 °C

Gas selectivity

The ideal gas selectivity for the combination of gases A and B (α(A/B)) is defined by the following equation [38]:

$$\alpha(\mathrm{A/B}) = \frac{P(\mathrm{A})}{P(\mathrm{B})} = \frac{D(\mathrm{A})}{D(\mathrm{B})} \times \frac{S(\mathrm{A})}{S(\mathrm{B})} = \alpha^{\mathrm{D}}(\mathrm{A/B}) \times \alpha^{\mathrm{S}}(\mathrm{A/B}) \quad (7)$$

where α^{D}(A/B) is the diffusivity selectivity and α^{S}(A/B) is the solubility selectivity. The O_2/N_2 and CO_2/CH_4 selectivities of the PBO(6FAHP-IPC) and its hybrids are listed in Table 3. It is recognized that the ideal selectivity (α(A/B)) for given gas pairs essentially depends on the diffusivity selectivity (α^{D}(A/B)) rather than the solubility selectivity (α^{S}(A/B)), which is consistent with a general understanding of the gas separation behavior of glassy polymers [38]. For

Table 3 O_2/N_2 and CO_2/CH_4 separation abilities of PBO(6FAHP-IPC)–silica hybrid membranes measured at 25 °C

Preparation temperature (°C)	SiO_2 content (wt%)	O_2/N_2 separation			CO_2/CH_4 separation		
		$\alpha(O_2/N_2)$	$\alpha^D(O_2/N_2)$	$\alpha^S(O_2/N_2)$	$\alpha(CO_2/CH_4)$	$\alpha^D(CO_2/CH_4)$	$\alpha^S(CO_2/CH_4)$
400	0	5.5	3.8	1.5	53	10	5.1
	10	5.4	4.6	1.2	51	9.5	5.4
	20	5.4	4.4	1.2	57	9.9	5.8
	30	5.1	4.2	1.2	57	8.7	6.5
420	0	5.4	3.7	1.5	48	9.1	5.3
	10	5.2	4.0	1.3	50	9.1	5.5
	20	4.9	3.9	1.3	49	8.2	5.8
	30	4.9	4.0	1.2	54	8.9	6.5
450	0	4.5	4.0	1.1	37	8.8	4.1
	10	4.4	3.8	1.1	38	8.7	4.3
	20	4.1	3.4	1.2	39	8.0	4.9

CO_2/CH_4 separation, an interesting behavior is observed. The obtained $\alpha(CO_2/CH_4)$ is plotted against the CO_2 permeability coefficient in Fig. 7. As shown in Fig. 7, the $\alpha(CO_2/CH_4)$ values of each hybrid prepared by the corresponding thermal treatment increase with increasing CO_2 permeability, tending to cross the upper bound for CO_2/CH_4 separation [39, 40]. This behavior is not in accordance with the general trend that glassy polymers that are more permeable are less selective and vice versa [38]. Considering the difference in the kinetic diameter between CO_2 (3.3 Å) and CH_4 (3.87 Å) [38] and the maintained CO_2/CH_4 diffusivity selectivity, $\alpha^D(CO_2/CH_4)$, of the hybrid membranes shown in Table 3, the improved CO_2/CH_4 separation ability might be brought by characteristic free volume holes, which accelerate a size-selective CO_2/CH_4 separation ability, created around the polymer/silica interfacial area. In addition, it should be mentioned that 400 °C- and 420 °C-treated hybrids containing 30 wt% silica and 450 °C-treated hybrids possess high CO_2/CH_4 separation ability that exceeds the upper bound updated in 2008. In particular, the $\alpha(CO_2/CH_4)$ value of the 450 °C-treated hybrid containing 20 wt% silica shows 21% improvement against the value expected from the upper bound established in 2008. The prominent CO_2/CH_4 separation ability might be achieved by the synergistic effects of (1) characteristic free volume holes created around the polymer/silica interfacial area brought on by the hybridization with silica and (2) the enhanced intermolecular chain distance and free volume holes due to the thermal treatment, which accelerate a size-selective CO_2/CH_4 separation ability. Even though the PBO(6FAHP-IPC)–silica hybrids cannot thus far exceed the advanced trade-off line of CO_2/CH_4 separation for existing TR-polymers including TR-PBOs (Fig. 7) [40, 41], it can be said that the PBO(6FAHP-IPC)–silica hybrids prepared by different thermal treatment protocols have a potentially attractive CO_2/CH_4 separation ability.

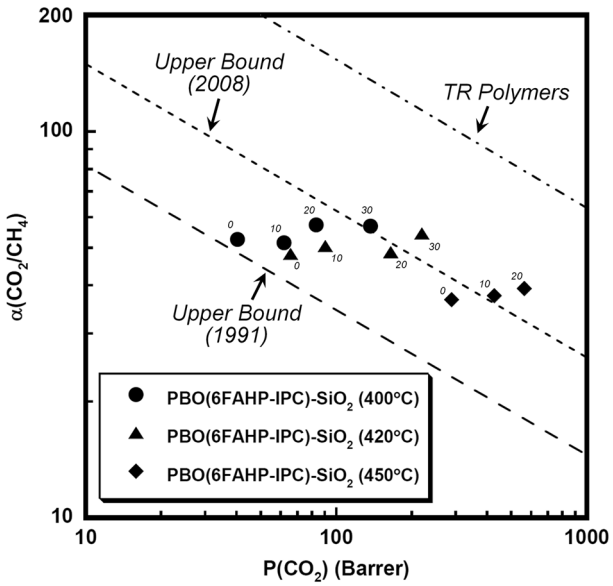

Fig. 7 Ideal CO_2/CH_4 selectivity of PBO(6FAHP-IPC)–silica hybrid membranes plotted against the CO_2 permeability coefficient measured at 25 °C; the attached number represents the silica content (wt%) in the membrane

Conclusion

The gas transport properties of PBO(6FAHP-IPC)–silica hybrid membranes prepared via a sol–gel reaction and different thermal treatment protocols were investigated. The thermal decomposition and glass transition temperatures of the hybrids increase with increasing silica content, indicating improved thermal stability by hybridization with silica. The gas permeability of the hybrids increases with increasing silica content, suggesting the formation of free volume holes around the polymer/silica interfacial area. The gas permeability of the PBO(6FAHP-IPC) and its hybrids are further increased with increasing thermal treatment temperature due to an increased intermolecular chain distance and FFV. In particular, the 450 °C-treated hybrids show both high CO_2 permeability and an excellent CO_2/CH_4 separation ability, which exceeds the upper bound for CO_2/CH_4 separation established in 2008. The noticeable CO_2/CH_4 separation ability might be achieved by the synergistic effects of (1) characteristic free volume holes created around the polymer/silica interfacial area brought on by the hybridization with silica and (2) the enhanced intermolecular chain distance and free volume holes due to the increased treatment temperature. With the simultaneous application of hybridization and thermal treatment techniques, the development of PBO-based high-performance gas separation membranes with attractive gas permeability and/or selectivity would be expected.

Acknowledgements This work was supported by JSPS KAKENHI Grant Number JP17K05994.

Compliance with ethical standards

Conflict of interest The authors declare that they have no competing interests.

Publisher's note: Springer Nature remains neutral with regard to jurisdictional claims in published maps and institutional affiliations.

References

1. Bernardo P, Drioli E, Golemme G. Membrane gas separation: a review/state of the art. Ind Eng Chem Res. 2009;48:4638–63.
2. Yampolskii Y. Polymeric gas separation membranes. Macromolecules. 2012;45:3298–311.
3. Robeson LM, Smith ZP, Freeman BD, Paul DR. Contributions of diffusion and solubility selectivity to the upper bound analysis for glassy gas separation membranes. J Membr Sci. 2014;453:71–83.
4. Chung TS, Jiang LY, Li Y, Kulprathipanja S. Mixed matrix membranes (MMMs) comprising organic polymers with dispersed inorganic fillers for gas separation. Prog Polym Sci. 2007;32:483–507.
5. Zhang Y, Sunarso J, Liu S, Wang R. Current status and development of membranes for CO_2/CH_4 separation: a review. Int J Greenh Gas Control. 2013;12:84–107.
6. Sanders DF, Smith ZP, Guo R, Robeson LM, McGrath JE, Paul DR, et al. Energy-efficient polymeric gas separation membranes for a sustainable future: a review. Polymer. 2013;54:4729–61.
7. Li Y, Wang X, Ding M, Xu J. Effect of molecular structure on the permeability and permselectivity of aromatic polyimides. J Appl Polym Sci. 1996;61:741–8.
8. Suzuki T, Yamada Y, Tsujita Y. Gas transport properties of 6FDA-TAPOB hyperbranched polyimide membrane. Polymer. 2004;45:7167–71.
9. Scholes CA, Freeman BD. Thermal rearranged poly(imide-co-ethylene glycol) membranes for gas separation. J Membr Sci. 2018;563:676–83.
10. Sanaeepur H, Amooghin AE, Bandehali S, Moghadassi A, Matsuura T, Van der Bruggen B. Polyimides in membrane gas separation: monomer's molecular design and structural engineering. Prog Polym Sci. 2019;91:80–125.
11. Park HB, Jung CH, Lee YM, Hill AJ, Pas SJ, Mudie ST, et al. Polymers with cavities tuned for fast selective transport of small molecules and ions. Science. 2007;318:254–8.
12. Jo HJ, Soo CY, Dong G, Do YS, Wang HH, Lee MJ, et al. Thermally rearranged poly(benzoxazole-co-imide) membranes with superior mechanical strength for gas separation obtained by tuning chain rigidity. Macromolecules. 2015;48:2194–202.
13. Alghunaimi F, Ghanem B, Wang Y, Salinas O, Alaslai N, Pinnau I. Synthesis and gas permeation properties of a novel thermally rearranged polybenzoxazole made from an intrinsically microporous hydroxyl-functionalized triptycene-based polyimide precursor. Polymer. 2017;121:9–16.
14. Cornelius CJ, Marand E. Hybrid silica-polyimide composite membranes: gas transport properties. J Membr Sci. 2002;202:97–118.
15. Chen K, Xu K, Xiang L, Dong X, Han Y, Wang C, et al. Enhanced CO_2/CH_4 separation performance of mixed-matrix membranes through dispersion of sorption-selective MOF nanocrystals. J Membr Sci. 2018;563:360–70.
16. Amooghin AE, Mashhadikhan S, Sanaeepur H, Moghadassi A, Matsuura T, Ramakrishna S. Substantial breakthroughs on function-led design of advanced materials used in mixed matrix membranes (MMMs): a new horizon for efficient CO_2 separation. Prog Mater Sci. 2019;102:222–95.
17. Suzuki T, Yamada Y, Itahashi K. 6FDA-TAPOB hyperbranched polyimide-silica hybrids for gas separation membranes. J Appl Polym Sci. 2008;109:813–9.
18. Suzuki T, Takenaka M, Yamada Y. Synthesis and gas transport properties of hyperbranched polybenzoxazole—silica hybrid membranes. J Membr Sci. 2017;521:10–17.
19. Suzuki T, Otsuki Y. Gas transport properties of polybenzoxazole–silica hybrid membranes prepared with different alkoxysilanes. Polym J. 2018;50:177–86.
20. Wang H, Chung TS. The evolution of physicochemical and gas transport properties of thermally rearranged polyhydroxyamide (PHA). J Membr Sci. 2011;385-6:86–95.
21. Imai Y, Itoya K, Kakimoto M. Synthesis of aromatic polybenzoxazoles by silylation method and their thermal and mechanical properties. Macromol Chem Phys. 2000;201:2251–6.
22. Oishi Y, Konno A, Oravec J, Mori K. Synthesis and properties of fluorine-containing polybenzoxazoles by in situ silylation method. J Photopolym Sci Technol. 2006;19:669–72.
23. Miyata S, Sato S, Nagai K, Nakagawa T, Kudo K. Relationship between gas transport properties and fractional free volume determined from dielectric constant in polyimide films containing the hexafluoroisopropylidene group. J Appl Polym Sci. 2008;107:3933–44.
24. Muruganandam N, Koros WJ, Paul DR. Gas sorption and transport in substituted polycarbonates. J Polym Sci B Polym Phys. 1987;25:1999–2026.
25. Morisato A, Shen HC, Sankar SS, Freeman BD, Pinnau I, Casillas CG. Polymer characterization and gas permeability of poly(1-trimethylsilyl-1-propyne) [PTMSP], poly(1-phenyl-1-propyne) [PPP], and PTMSP/PPP blends. J Polym Sci B Polym Phys. 1996;34:2209–22.
26. Weinkauf DH, Kim HD, Paul DR. Gas transport properties of liquid crystalline poly(p-phenyleneterephthalamide). Macromolecules. 1992;25:788–96.
27. van Krevelen DW. Properties of polymers. 3rd ed. Amsterdam, The Netherlands: Elsevier; 1990.
28. Park JY, Paul DR. Correlation and prediction of gas permeability in glassy polymer membrane materials via a modified free volume based group contribution method. J Membr Sci. 1997;125:23–39.
29. Luo S, Liu J, Lin H, Kazanowska BA, Hunckler MD, Roeder RK, et al. Preparation and gas transport properties of triptycene-containing polybenzoxazole (PBO)-based polymers derived from thermal rearrangement (TR) and thermal cyclodehydration (TC) processes. J Mater Chem A. 2016;4:17050–62.
30. Hsiao SH, Huang YH. A new class of aromatic polybenzoxazoles containing ortho-phenylenedioxy groups. Eur Polym J. 2004;40:1127–35.
31. Kudo H, Maruyama K, Shindo S, Nishikubo T, Nishimura I. Syntheses and properties of hyperbranched polybenzoxazole by thermal cyclodehydration of hyperbranched poly[o-(t-butoxycarbonyl)amide] via A_2+B_3 approach. J Polym Sci A Polym Chem. 2006;44:3640–9.
32. Hibshman C, Cornelius CJ, Marand E. The gas separation effects of annealing polyimide—organosilicate hybrid membranes. J Membr Sci. 2003;211:25–40.
33. Zhu H, Ma Y, Fan Y, Shen J. Fourier transform infrared spectroscopy and oxygen luminescence probing combined study of modified sol–gel derived film. Thin Solid Films. 2001;397:95–101.
34. Han SH, Kwon HJ, Kim KY, Seong JG, Park CH, Kim S, et al. Tuning microcavities in thermally rearranged polymer membranes for CO_2 capture. Phys Chem Chem Phys. 2012;14:4365–73.

35. Nafisi V, Hägg MB. Development of nanocomposite membranes containing modified Si nanoparticles in PEBAX-2533 as a block copolymer and 6FDA-durene diamine as a glassy polymer. Appl Mater Interfaces. 2014;6:15643–52.
36. Hasebe S, Aoyama A, Tanaka M, Kawakami H. CO_2 separation of polymer membranes containing silica nanoparticles with gas permeable nano-space. J Membr Sci. 2017;536:148–55.
37. Japip S, Wang H, Xiao Y, Chung TS. Highly permeable zeolitic imidazolate framework (ZIF)-71 nano-particles enhanced polyimide membranes for gas separation. J Membr Sci. 2014;467:162–74.
38. Freeman BD. Basis of permeability/selectivity tradeoff relations in polymeric gas separation membranes. Macromolecules. 1999; 32:375–80.
39. Robeson LM. Correlation of separation factor versus permeability for polymeric membranes. J Membr Sci. 1991;62:165–85.
40. Robeson LM. The upper bound revisited. J Membr Sci. 2008; 320:390–400.
41. Han SH, Misdan N, Kim S, Doherty CM, Hill AJ, Lee YM. Thermally rearranged (TR) polybenzoxazole: effects of diverse imidization routes on physical properties and gas transport behaviors. Macromolecules. 2010;43:7657–67.